TECHNICAL PAPER

ISSN:1047-3289 *J. Air & Waste Manage. Assoc.* **59**:1049–1060
DOI:10.3155/1047-3289.59.9.1049

Using High Time Resolution Aerosol and Number Size Distribution Measurements to Estimate Atmospheric Extinction

William C. Malm
National Park Service, Cooperative Institute for Research in the Atmosphere, Colorado State University, Fort Collins, CO

Gavin R. McMeeking, Sonia M. Kreidenweis, Ezra Levin, and Christian M. Carrico
Department of Atmospheric Science, Colorado State University, Fort Collins, CO

Derek E. Day
Cooperative Institute for Research in the Atmosphere, Colorado State University, Fort Collins, CO

Jeffrey L. Collett, Jr., Taehyoung Lee, Amy P. Sullivan, and Suresh Raja
Department of Atmospheric Science, Colorado State University, Fort Collins, CO

ABSTRACT

Rocky Mountain National Park is experiencing reduced visibility and changes in ecosystem function due to increasing levels of oxidized and reduced nitrogen. The Rocky Mountain Atmospheric Nitrogen and Sulfur (RoMANS) study was initiated to better understand the origins of sulfur and nitrogen species as well as the complex chemistry occurring during transport from source to receptor. As part of the study, a monitoring program was initiated for two 1-month time periods—one during the spring and the other during late summer/fall. The monitoring program included intensive high time resolution concentration measurements of aerosol number size distribution, inorganic anions, and cations, and 24-hr time resolution of $PM_{2.5}$ and PM_{10} mass, sulfate, nitrate, carbon, and soil-related elements concentrations. These data are combined to estimate high time resolution concentrations of $PM_{2.5}$ and PM_{10} aerosol mass and fine mass species estimates of ammoniated sulfate, nitrate, and organic and elemental carbon. Hour-by-hour extinction budgets are calculated by using these species concentration estimates and measurements of size distribution and assuming internal and external particle mixtures. Summer extinction was on average about 3 times higher than spring extinction. During spring months, sulfates, nitrates, carbon mass, and $PM_{10} - PM_{2.5}$ mass contributed approximately equal amounts of extinction, whereas during the summer months, carbonaceous material extinction was 2–3 times higher than other species.

IMPLICATIONS

The Regional Haze Rule requires the nation to make progress toward the goal of natural visibility conditions in certain federally protected lands on the 20% haziest days. The measurements that track progress toward this goal are based on 24-hr particulate measurements. At Rocky Mountain National Park, it is shown that 24-hr measurements are made up of short temporal excursions consisting of only a few hours that are 2–5 times greater than the average. On a 24-hr average, ammonium nitrate may never contribute to the 20% haziest days; however, for periods of hours, it could contribute significantly to the worst visibility conditions.

INTRODUCTION

Atmospheric nitrogen and sulfur species can cause several deleterious effects, including visibility impairment and changes in ecosystem function and surface water chemistry from atmospheric deposition. In Rocky Mountain National Park (RMNP), the most recent 12-yr-average winter fractional contributions of nitrates and sulfates to visibility impairment are 18 and 36%, respectively. However, during some days, nitrates can contribute over 50%, whereas on other days sulfates contribute over 60% to particle light extinction. Although atmospheric concentrations of sulfur species have decreased in recent years, nitrogen concentrations have not. In fact, ambient nitrate concentrations have increased by approximately 10–20% over the past 10 yr. Nitrate wet deposition has increased by approximately the same amount, and ammonium wet deposition has increased by approximately 50%.

The Rocky Mountain Atmospheric Nitrogen and Sulfur study (RoMANS) was initiated to better understand the origins and physical, chemical, and optical characteristics of sulfur and nitrogen species, as well as the complex chemistry occurring during transport from source to receptor.

As part of the study, a monitoring program was conducted over two time periods—one in the spring and the other during late summer/fall—that were approximately 1

Table 1. Measurements at the core site.

Measurement	Instrument	Time Resolution	Notes
$PM_{2.5}$ inorganic ions and gases	Annular denuder/filter pack sampler (URG)[1,2]	24 hr	Cl^-, NO_2^-, NO_3^-, SO_4^{2-}, Na^+, K^+, NH_4^+, Mg^{2+}, Ca^{2+}, HNO_3, NH_3
$PM_{2.5}$ inorganic ions	PILS–IC[3–5]	15 min	Cl^-, NO_2^-, NO_3^-, SO_4^{2-}, Na^+, K^+, NH_4^+, Mg^{2+}, Ca^{2+}
$PM_{2.5}$ mass, ions, elements, H, and OC/LAC	IMPROVE sampler	24 hr	Components per IMPROVE protocol
PM_{10} mass, ions, elements, and OC/LAC	IMPROVE sampler	24 hr	Components per IMPROVE protocol
SO_2, NO_x, NH_3, CO, O_3	Various continuous gas monitors	15 min	NH_3 detection limit higher than for denuder method
Meteorological parameters	Met station	2 min	T, RH, WD, WS, precipitation, SR, BP
Particle size distributions	Differential mobility particle sizing (DMPS) system, optical particle counter (OPC), and aerodynamic particle sizer (APS)[6–10]	15 min	0.05–15 μm diameter
Particle light scattering	Optec open air nephelometer	2 min	Ambient aerosol

Notes: IC = ion chromatography, NO_2^- = nitrite ion, T = temperature, WD = wind direction, WS = wind speed, SR = solar radiation, BP = barometric pressure.

mo in duration. The monitoring program consisted of intensive, high time resolution measurements of particles, gas, wet deposition, and meteorology at a core site in RMNP; daily time resolution measurements at two secondary sites to characterize air masses on east and west slopes; and additional monitoring that focused primarily on weekly ammonia (NH_3) measurements at sites throughout the state of Colorado and near state boundaries.

This paper will focus on the high time resolution temporal variability of several variables derived from the particle number size distributions (NSDs) covering the size range from 0.05 to 15 μm, $PM_{2.5}$ semicontinuous inorganic species measurements, 24-hr average $PM_{2.5}$ inorganic and organic species, and particle light scattering. Biases between semicontinuous and 24-hr average concentration measurements of inorganic species are explored, and high time resolution organic mass concentrations are derived from measurements of inorganic species and particle NSDs. Finally, the high time resolution data are used to estimate particle scattering and absorption, which in turn are compared with measured scattering.

MONITORING PROGRAM

Two 1-month intensive sampling periods were conducted in 2006 during time periods that typically are associated with precipitation events. One sampling period occurred between February and April, when synoptically driven upslope flow events are likely to occur, resulting in snow and/or rain events in the Rocky Mountains and likely contributions of pollutants from the Front Range areas and surrounding regions. The second sampling period occurred between July and August. A summary of the measurements is included in Table 1 and monitoring locations are shown in Figure 1.

Measurements were made at a core site located within RMNP, at two secondary sites (one located on the western slope of RMNP and one on the Front Range), and at an array of approximately 20 satellite sites located across eastern Colorado and on the western slope. As illustrated in Table 1, the most sophisticated suite of measurements and the highest time resolution measurements were made at the RMNP core site. It is this dataset that is used in the analysis presented here.

Measurements for the RMNP core site included detailed observations of $PM_{2.5}$ and PM_{10} particle composition, ion size distributions, trace gas concentrations (including sulfur dioxide [SO_2], oxides of nitrogen [NO_x], NH_3, nitric acid [HNO_3], carbon monoxide [CO], and ozone [O_3]), wet deposition, cloud water composition, particle size distributions, particle light scattering, and meteorology. Time-integrated and high time resolution (at least hourly) measurements were made for nearly all measurement parameters at the core site. Measurements at the two secondary sites were focused primarily on concentrations of key particle species, key trace gases, and wet deposition.

DATA ANALYSIS

Compliance under the Regional Haze Rule is based on protocols for reconstructing aerosol mass concentrations and light extinction coefficients (b_{ext}). Reconstruction equations are used to estimate $PM_{2.5}$ mass concentrations (for particles with aerodynamic diameters <2.5 μm) as well as light extinction coefficients. Dry $PM_{2.5}$ fine mass is computed with eq 1 on the basis of assumed components.

$$PM_{2.5} = (NH_4)_2SO_4 + NH_4NO_3 + POM + LAC + Soil + SS \quad (1)$$

In this form, sulfate is assumed to be fully neutralized ammonium sulfate ($(NH_4)_2SO_4$), nitrate is assumed to be in the form of ammonium nitrate (NH_4NO_3), and organic carbon (OC) is included as particulate organic material (POM), computed by multiplying OC concentrations by a molecular weight per carbon weight ratio ($POM = R_{oc} \times OC$), where R_{oc} is 1.8.[11] Light-absorbing carbon is referred to as LAC. The authors use the term LAC because it is more representative of the optical properties of absorbing carbon than elemental (elemental carbon [EC]) or black carbon (BC), although these terms are often used interchangeably in the literature. $PM_{2.5}$ soil concentrations

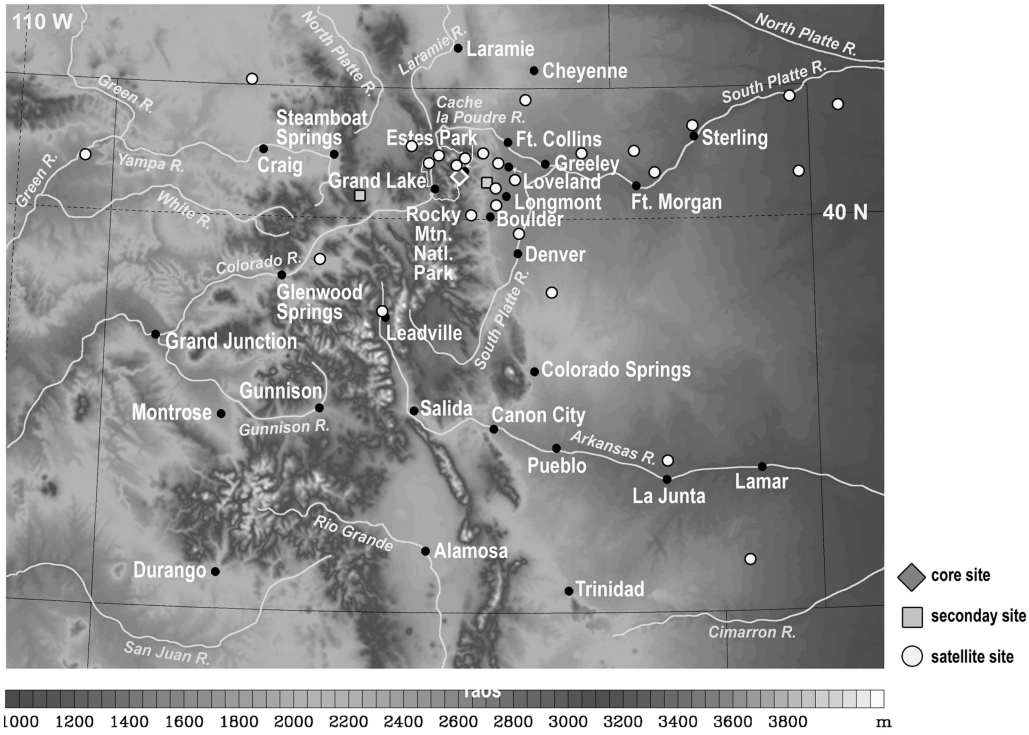

Figure 1. Map showing monitoring locations of the core site (◇), secondary (□) and satellite sites (○).

include the contributions from the following assumed forms of elemental species (eq 2).[12] Mass concentrations are given in units of $\mu g \cdot m^{-3}$.

$$\text{Soil} = 2.2\text{A1} + 2.49\text{Si} + 1.94\text{Ti} + 1.63\text{Ca} + 2.42\text{Fe} \quad (2)$$

where *SS* refers to sea salt and is estimated as $SS = 1.8 \times Cl^-$, where Cl^- is the chloride concentration.

Closure between the Sum of Measured Fine and Coarse Mass Species and Gravimetric Mass Concentrations

Table 2, a and b, shows statistical summaries of 24-hr average $PM_{2.5}$ gravimetric mass, $(NH_4)_2SO_4$ and NH_4NO_3, OC and EC, soil, and sea salt at the core site as measured using the Interagency Monitoring of Protected Visual Environments (IMPROVE) sampling system during the spring and summer field campaigns. Table 3, a and b, shows the same summaries for the $PM_{10} - PM_{2.5}$ measurements. The fourth column in each table is the fraction of each variable compared with reconstructed mass.

Figure 2 shows scatterplots of reconstructed $PM_{2.5}$ versus gravimetric mass for spring and summer datasets. For an ordinary least square (OLS) regression between reconstructed and measured $PM_{2.5}$ mass with the intercept set to zero, the R^2 values for the spring and summer scatterplots are 0.93 and 0.98, respectively, with slopes of 1.11 ± 0.02 and 0.95 ± 0.01. The regression and the average ratio of gravimetric to measured $PM_{2.5}$ mass show that reconstructed mass is approximately 10–15% high in the spring and 5% low in the summer. Despite the many assumptions of the chemical forms of each species, the agreement between the two variables is quite good. Comparison of reconstructed and gravimetric mass for $PM_{10} - PM_{2.5}$ shows that the agreement is less robust. During the spring and summer

Table 2a. Statistical summary of aerosol species derived from the IMPROVE $PM_{2.5}$ monitoring system for the spring campaign.

Variable	Mean	SD	Fraction	Min	Max
$PM_{2.5}$	2.51	1.45	0.87	0.27	6.15
$PM_{2.5recon}$	2.90	1.45		0.72	6.09
$(NH_4)_2SO_4$	0.66	0.36	0.23	0.16	1.76
NH_4NO_3	0.35	0.44	0.12	0.01	1.65
POM	0.88	0.36	0.30	0.31	1.69
LAC	0.09	0.07	0.03	0.02	0.30
Soil	0.91	0.73	0.31	0.08	3.69
Sea salt	0.01	0.01	0.00	0.00	0.03

Notes: The number of data points is 37. Units are in $\mu g/m^3$.

Table 2b. Statistical summary of aerosol species derived from the IMPROVE $PM_{2.5}$ monitoring system for the summer campaign.

Variable	Mean	SD	Fraction	Min	Max
$PM_{2.5}$	5.57	2.18	1.02	1.15	12.46
$PM_{2.5recon}$	5.47	2.11		1.37	12.39
$(NH_4)_2SO_4$	0.90	0.26	0.16	0.21	1.67
NH_4NO_3	0.16	0.15	0.03	0.04	0.53
POM	3.20	1.62	0.58	0.94	9.10
LAC	0.24	0.10	0.04	0.06	0.54
Soil	0.97	0.53	0.18	0.04	1.84
Sea salt	0.00	0.00	0.00	0.00	0.01

Notes: Units are in $\mu g/m^3$.

Table 3a. Statistical summary of aerosol species derived from the IMPROVE $PM_{10} - PM_{2.5}$ monitoring system for the spring campaign.

Variable	Mean	SD	Fraction	Min	Max
$PM_{10} - PM_{2.5}$	2.45	1.62	0.80	−0.10	7.58
$(PM_{10} - PM_{2.5})_{recon}$	3.06	2.16		−0.21	10.19
$(NH_4)_2SO_4$	0.07	0.04	0.02	0.00	0.18
NH_4NO_3	0.15	0.10	0.05	0.00	0.45
POM	0.43	0.36	0.14	−0.07	1.44
LAC	0.03	0.06	0.01	−0.08	0.14
Soil	2.37	1.86	0.77	−0.19	9.02
Sea salt	0.02	0.02	0.01	0.00	0.10

Notes: The number of data points is 37. Units are in $\mu g/m^3$.

Table 3b. Statistical summary of aerosol species derived from the IMPROVE $PM_{10} - PM_{2.5}$ monitoring system for the summer campaign.

Variable	Mean	SD	Fraction	Min	Max
$PM_{10} - PM_{2.5}$	4.14	2.46	0.84	−0.55	9.03
$(PM_{10} - PM_{2.5})_{recon}$	4.94	2.45		0.59	9.46
$(NH_4)_2SO_4$	0.03	0.04	0.01	−0.05	0.12
NH_4NO_3	0.16	0.11	0.03	0.05	0.48
POM	1.30	0.45	0.26	0.17	2.03
LAC	0.06	0.06	0.01	−0.03	0.23
Soil	3.36	2.15	0.68	−0.28	7.41
Sea salt	0.02	0.04	0.00	0.00	0.19

Notes: The number of data points is 35. Units are in $\mu g/m^3$.

campaigns, reconstructed mass is 25 and 68% greater, respectively, than gravimetric $PM_{10} - PM_{2.5}$. An OLS regression between gravimetric mass as the dependent variable and the various species as independent variables suggests that $PM_{10} - PM_{2.5}$ soil and POM concentrations are being overestimated.

Referring to Tables 2 and 3, one can see that $PM_{2.5}$ and $PM_{10} - PM_{2.5}$ mass are about a factor of 2 higher in the summer than spring. The differences in mass concentrations are primarily due to POM concentrations being approximately 3.5 times greater during the summer than spring. Conversely, $PM_{2.5}$ nitrate concentrations are approximately 2 times greater in the spring than summer; however, they make up a smaller percentage of reconstructed mass at 12 and 3%, respectively, for the summer and spring months. During the summer campaign, organic mass made up 60% of the $PM_{2.5}$ mass, with $(NH_4)_2SO_4$ and soil each contributing approximately 15%. During the spring season, sulfates, POM, and soil made up about equal fractions of $PM_{2.5}$ at approximately 30%. The $PM_{10} - PM_{2.5}$ mass fraction was dominated by soil at approximately 75% for both seasons, and organics were the second largest contributor at 24 and 14% for the summer and spring seasons, respectively.

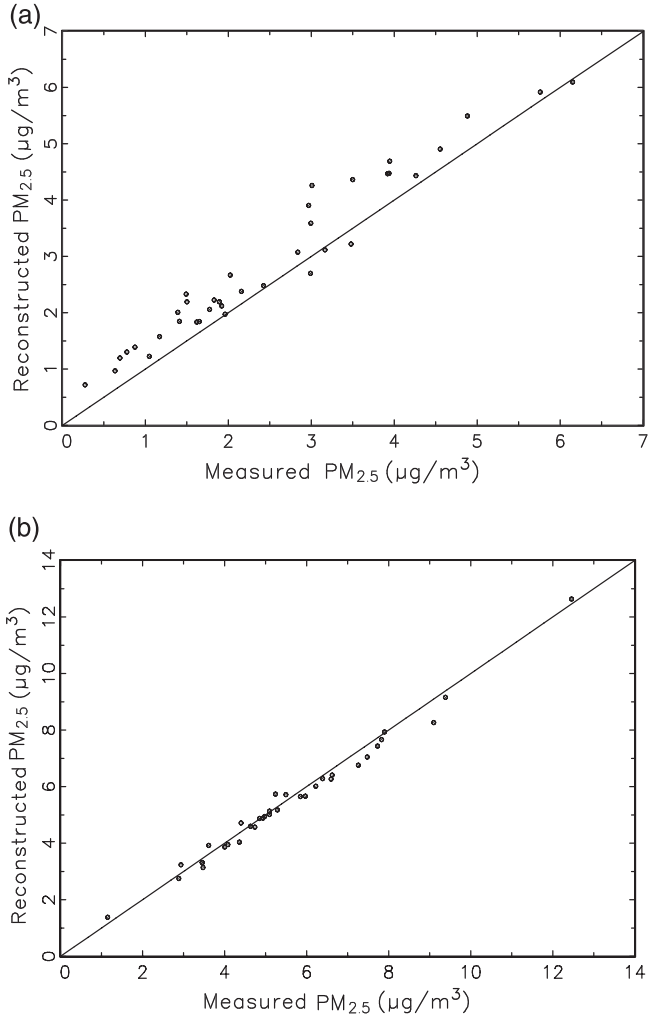

Figure 2. Reconstructed vs. gravimetric mass for (a) spring and (b) summer.

Comparison of Semicontinuous to 24-hr Average Measurements of Inorganic Aerosols

The particle-into-liquid sampler (PILS)[3] was operated continuously during the two campaigns to obtain the concentrations of major ions (ammonium $[NH_4^+]$, sodium $[Na^+]$, potassium $[K^+]$, calcium $[Ca^{2+}]$, magnesium $[Mg^{2+}]$, chloride $[Cl^-]$, nitrate $[NO_3^-]$, and sulfate $[SO_4^{2-}]$) with a time resolution of 15 min. However, all 15-min data were averaged to 1 hr for the analysis presented here. The performance of the PILS system is evaluated by comparing its measurements of various species to those collected using 24-hr bulk sampling techniques.

As an example, Figure 3a shows a temporal plot of NO_3^- mass concentrations as collected by the semicontinuous PILS and URG Corp.[1,2] 24-hr average measurement for the spring, whereas Figure 3b is a scatterplot of URG NO_3 versus IMPROVE NO_3^- and 24-hr average PILS NO_3^-. Table 4 is a statistical summary of NO_3^-, SO_4^{2-}, and NH_4^+ concentrations, measured using the IMPROVE, URG, and PILS measurement systems, for spring and summer.

As indicated in Figure 3b and Table 4, all of the measurements of the NO_3^-, including PILS, agree reasonably well. On average during the spring season, the average PILS NO_3^- measurement is 20% less than the URG but similar to IMPROVE, whereas during the summer PILS measurements are approximately 25 and 40% greater than URG and IMPROVE, respectively. Measurements of SO_4^{2-} concentrations by PILS are 10–30% greater than URG measurements for spring and summer, respectively, but 20–30% less for NH_4^+ measurements.

For the most part, the IMPROVE and URG measurements compare favorably. In spring and summer months

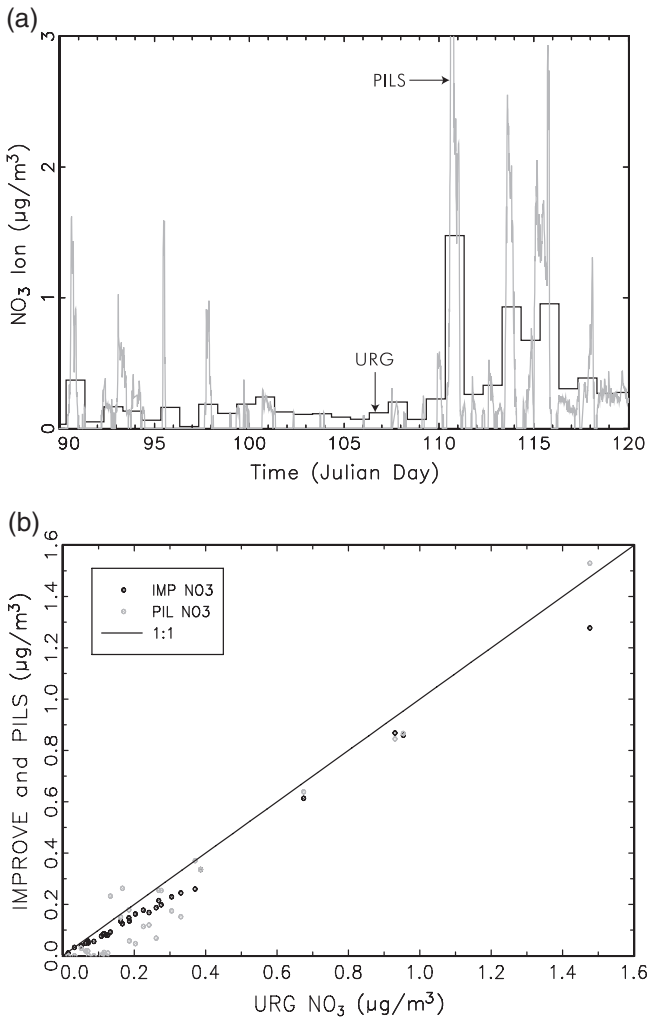

Figure 3. (a) Time series of NO_3^- mass concentrations for the semicontinuous PILS 24-hr-average URG measurement systems. (b) Scatterplot of 24-hr average NO_3^- measurements made by the IMPROVE and PILS system on the *y*-axis and the URG-measured NO_3^- on the *x*-axis.

the NO_3^- concentrations as derived from the URG are greater than IMPROVE by 18 and 13%, respectively, whereas the difference between the corresponding SO_4^{2-} measurements is only approximately 4%. For purposes of calculations made in the remainder of this paper, PILS NO_3^- and SO_4^{2-} data were normalized to URG data in increments of 24 hr.

The most striking feature of Figure 3 is the extreme, short time scale variability of NO_3^- concentrations. Any 24-hr bulk measured concentration is typically made up of short-term episodes that are 12 hr or less in duration. The variability of the average 24- versus 1-hr data can be assessed by comparing the statistical summaries of the various datasets in which maximum, minimum, and standard deviations of the various variables are shown (Table 4). The 24-hr average maximum NO_3^- concentration for the data shown in Figure 3 is 1.48 $\mu g/m^3$, whereas the maximum 1-hr concentration is 4.95 $\mu g/m^3$, a factor of 3.3 higher. The standard deviation of the 1-hr dataset is 0.5, whereas for the 24-hr average dataset it is 0.32, a factor of 1.7 times higher. Plots of SO_4^{2-} and NH_4^+ are similar to Figure 3 for the spring and summer months.

The implication of the high temporal variability in aerosol concentrations on visibility is very significant. Because visibility impairment is an instantaneous phenomenon, the highly variable aerosol concentrations will result in visibility that is changing from a fairly high to a fairly low level of impairment within time scales of less than 1 hr. This issue will be further addressed in the section on atmospheric extinction estimates.

Aerosol Number Particle Size Distributions

Ambient aerosol was sampled through a flow splitter to deliver a common aerosol sample to the particle sizing instrumentation. Dry size distributions were measured with an electrical mobility technique (40 nm $< D <$ 850 nm using models 3081 and 3785 from TSI, Inc.), a time-of-flight technique (aerodynamic 0.6 $< D <$ 15 μm using model 3320 from TSI, Inc.), and an optical sizing technique (0.05 $< D <$ 2 μm using LASAIR 1002 and 1003 from Particle Measuring Systems, Inc.).[6–10] Aerosol drying was accomplished using Nafion membrane driers (Permapure, Inc.) for the optical and electrical mobility analyzers and heating (temperature ~35 °C) for time-of-flight measurements. One of the optical particle counters measured unconditioned aerosol from the flow splitter. Examination of the overlapping regions for

Table 4. Statistical summary of SO_4^{2-}, NO_3^-, and NH_4^+ measurements ($\mu g/m^3$) made by the IMPROVE, URG, and PILS measurement systems for spring and summer.

	Spring					Summer				
Variable	**Mean**	**SD**	**Min**	**Max**	***N***	**Mean**	**SD**	**Min**	**Max**	***N***
NO_3IMP	0.23	0.29	0.01	1.28	31	0.13	0.12	0.03	0.41	31
NO_3URG	0.28	0.32	0.01	1.48	31	0.15	0.14	0.03	0.52	31
NO_3PILS	0.22	0.52	0.00	4.95	738	0.19	0.30	0.00	3.59	727
SO_4IMP	0.49	0.28	0.11	1.28	31	0.68	0.17	0.27	1.21	31
SO_4URG	0.51	0.27	0.11	1.27	31	0.65	0.17	0.28	1.20	31
SO_4PILS	0.57	0.51	0.00	2.63	738	0.84	0.28	0.14	2.22	727
NH_4IMP	0.19	0.13	0.04	0.52	31	0.23	0.08	0.11	0.44	31
NH_4URG	0.30	0.14	0.13	0.65	31	0.33	0.14	0.12	0.78	31
NH_4PILS	0.23	0.35	0.00	2.08	738	0.24	0.16	0.00	1.42	727

Notes: IMP = IMPROVE, URG = URG Corp.

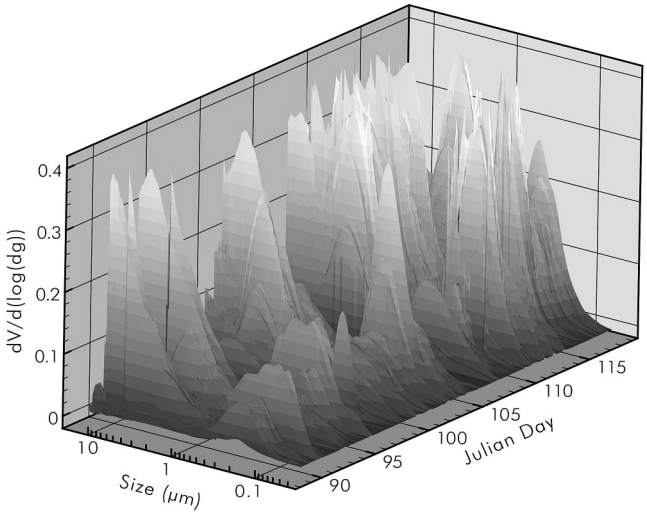

Figure 4. Three-dimensional contour plot of d*V*/day(log*D*) for spring.

these measurements yields information on the refractive index and density.[9,13,14]

Figure 4 is a plot of d(*V*)/day(log(*D*)) versus log(*D*) for the spring season dataset. *D* is particle aerodynamic diameter and *V* is the particle volume in increment d(log(*D*)). For purposes of this dataset, the fine mode refers to particles ≈0.05–0.8 μm, whereas the coarse mode corresponds to those particles ≈0.8–10 μm. In Table 5, the average volume mean diameters during both spring and summer months were nearly the same at approximately 0.2 μm, with geometric standard deviations of 1.73 and 1.61 for the spring and summer, respectively, although the gravimetric fine mass concentration was a factor of 2 higher during the summer. The coarse volume mode had an average geometric volume mean diameter of 3.4 μm for the spring and 4.6 μm for the summer, with similar geometric standard deviations of approximately 2. These fine mode size distributions are typical of other measurements made in western national parks but not of eastern parks.[15–17] Measurements of the fine mode size distribution in eastern parks tended to be shifted toward larger sizes but with similar geometric standard deviations.[17]

An interesting feature of the time series of the volume size distributions shown in Figure 4 is the occurrences of elevated coarse particle mass independent of the fine mass mode, implying that during those time periods, the source region for coarse mass is not the same as that for fine particles. It is also of interest to point out that the 2.5-μm cut point that is typically used to characterize "fine" particles in most if not all U.S. national monitoring networks is very near the mass mean diameter of the measured coarse mode, implying that a significant amount of "coarse" aerosol is being mischaracterized as fine particle mass.

Table 5. Statistical summary of volume mean diameter and geometric standard deviation for the fine (≈0.5–0.8 μm) and coarse (≈0.8–10.0 μm) modes for spring and summer.

	Variable	Mean	SD	Minimum	Maximum
Spring					
Fine	D_g	0.20	0.03	0.11	0.33
	σ_g	1.73	0.13	1.25	2.19
Coarse	D_g	3.41	1.14	1.85	8.24
	σ_g	2.00	0.16	1.41	2.46
Summer					
Fine	D_g	0.22	0.03	0.14	0.27
	σ_g	1.61	0.08	1.45	2.02
Coarse	D_g	4.56	0.71	2.43	8.17
	σ_g	1.94	0.10	1.49	2.36

Notes: The number of data points is 742 in spring and 642 in summer.

Table 6. Summary of the index of refraction and densities used for modeling scattering and absorption from differential mobility analyzer NSDs.

Species	Density (g·cm^{-3})	Index of Refraction
$(NH_4)_2SO_4$	1.76[18]	1.53[18]
POM	1.4[19]	1.55[20]
EC	2.0[21]	1.8 − 0.5[21]
NH_4NO_3	2.26[18]	1.59[18]
Soil	2.3	2 (based on values reported in Hand and Kreidenweis, 2002[13])

Comparison of Average Fine and Coarse Particle Density Derived from Size Distribution Data to Those Estimated from 24-hr Average Species Mass Concentration Measurements

The volume size distribution data are used to estimate POM on a semicontinuous basis by differencing the fine mass estimates derived from the size distributions and the inorganic mass species obtained from the PILS monitoring system. Carrying out this calculation requires assumptions of fine and coarse mass chemical composition and the associated densities of each species. Typical densities and indices of refraction used for $(NH_4)_2SO_4$, NH_4NO_3, OC, EC, and soil are summarized in Table 6.

In Tables 2 and 3, it is evident that $PM_{2.5}$ is predominantly inorganic salts, POM, and soil dust, and that the coarse mode is overwhelmingly soil dust with a 10–20% contribution of organic material. This distribution of aerosol species between $PM_{2.5}$ and PM_{10} is typical.[22] Here, a differentiation is made between wind-entrained soil dust and soil-related elements emitted during the burning

Table 7. Statistical summary of volume-weighted densities (g/cm^3) for $PM_{2.5} - PM_{2.5}$soil, $PM_{10} - PM_{2.5} + PM_{2.5}$soil, and PM_{10} for spring and summer.

Variable	Mean	SD	Min	Max
Spring				
$\rho PM_{2.5} - PM_{2.5}$soil	1.63	0.07	1.50	1.82
$\rho PM_{10} - PM_{2.5} + PM_{2.5}$soil	2.15	0.18	1.77	2.80
ρPM_{10}	1.91	0.10	1.68	2.10
Summer				
$\rho PM_{2.5} - PM_{2.5\ soil}$	1.51	0.03	1.47	1.57
$\rho PM_{10} - PM_{2.5} + PM_{2.5}$soil	1.99	0.11	1.77	2.19
ρPM_{10}	1.75	0.11	1.58	1.98

Notes: The number of data points is 37 in spring and 35 in summer.

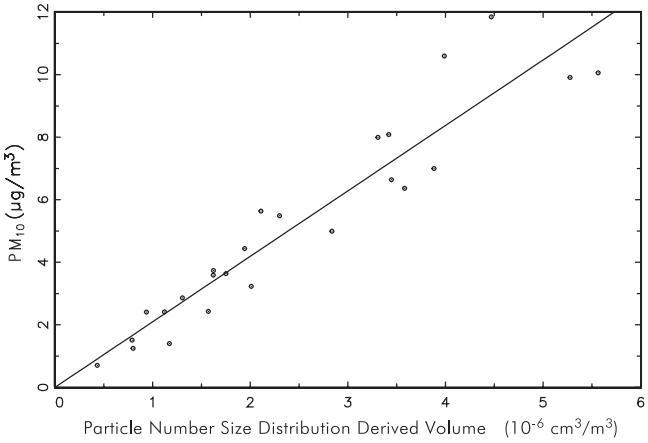

Figure 5. Scatterplot of PM_{10} mass concentrations ($\mu g/m^3$) vs. volume of fine + coarse particle volume per cubic meter of air as derived from the particle NSDs.

of carbonaceous material, whether it be coal- or forest/agriculture-related material. As such, it is usually assumed that the soil dust in the 0.0- to 2.5-μm size range is the fine "tail" of the coarse mode. Therefore it is assumed that the fine mode (0.05–0.8 μm) shown in Figure 4 is primarily made up of $(NH_4)_2SO_4$, NH_4NO_3, and POM. By estimating the slope of a scatterplot of particle volume and measured gravimetric fine mass an average fine mode density can be derived.

Table 7 is a statistical summary of volume-weighted densities for $PM_{2.5} - PM_{2.5}$soil, $PM_{10} - PM_{2.5} + PM_{2.5}$soil, and PM_{10}, derived from the individual species densities given in Table 6. If the assumption of volume conservation is approximately true and the individual species densities are correct, the volume-weighted densities should be comparable to the average densities derived from slope estimates of scatterplots of gravimetric mass versus volume as derived from the NSD measurements. An example scatterplot of 24-hr fine PM_{10} mass versus 24-hr average volume derived from the number distribution measurements is shown in Figure 5 for the spring dataset. The slope of the line, 2.09 ± 0.07 gm/cm^3, is interpreted as the average density of fine plus coarse particles over the measurement time period. The slope was

Table 8. Results of an OLS regression with the intercept set equal to zero for the dependent variable shown, with the independent variable being the corresponding volume derived from the NSD measurements.

Variable	Estimate	Standard Error	*t* value	> *t*
Spring				
$PM_{2.5} - PM_{2.5}$soil	1.60	0.09	18.50	0.00
$PM_{10} - PM_{2.5} + PM_{2.5}$soil	2.21	0.09	25.39	0.00
PM_{10}	2.09	0.07	28.82	0.00
Summer				
$PM_{2.5} - PM_{2.5}$soil	1.46	0.06	24.70	0.00
$PM_{10} - PM_{2.5} + PM_{2.5}$soil	1.87	0.17	10.74	0.00
PM_{10}	1.65	0.11	15.47	0.00

Notes: Units are in g/cm^3.

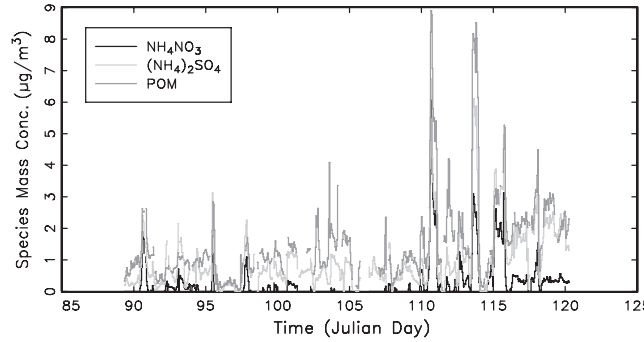

Figure 6. Time series of $(NH_4)_2SO_4$ and NH_4NO_3 measured using the PILS system and TCM derived from the particle size distribution data. Units are in $\mu g/m^3$.

determined using an OLS regression with the intercept set equal to zero.

Table 8 is a summary of the regressions carried out for total volume and volumes corresponding to the fine (≈0.05–0.8 μm) and coarse (≈0.8–10 μm) modes of volume size distribution data. The gravimetric fine mass was estimated using $PM_{2.5} - PM_{2.5}$soil, and coarse mode gravimetric mass was set equal to $PM_{10} - PM_{2.5} + PM_{2.5}$soil. Undoubtedly, some $PM_{10} - PM_{2.5}$ mode POM contributes to $PM_{2.5}$ organics, and $PM_{2.5}$soil-related elements may not all be associated with the coarse mode. Not correcting for the coarse POM in the fine mode will serve to somewhat inflate the fine mode density and underestimate the coarse-mode density. Furthermore, the gravimetric mass contains some water in that the filters are weighed at approximately 40 ± 5% relative humidity (RH) and hygroscopic species retain some water at these humidities.

The relative error between the two calculations for PM_{10} volumes and mass concentrations are 6 and 9% for the spring and summer months, respectively, with the volume-weighted density being smaller in the spring but larger in the summer. Interestingly, the relative errors for the individual fine and coarse modes were less at approximately 1–6%. The assumed species densities appear to be quite reasonable. Notice that because the fine mode on a relative basis has more POM than the coarse mode, its average density is lower than the coarse fraction, and vice versa for the coarse mode, which is dominated by soil dust with its higher density.

Estimating Semicontinuous Particulate Organic Mass from Mass Size Distributions

The fine and coarse mass associated with the NSDs can be estimated in various ways. One could assume the average density arrived at using the regression technique described above, use the average volume-weighted density derived from the bulk 24-hr average mass concentration data, or use each 24-hr time increment volume-weighted density derived from the 24-hr average data to estimate mass associated with the size distribution data in 24-hr increments. It is the latter approach that is used here.

Once the mass concentrations are estimated for the fine and coarse mode, the fine total carbon mass (TCM) concentrations, POM + LAC, can be estimated by differencing the mass concentrations derived from the NSD

measurements and the sum of $(NH_4)_2SO_4$ and NH_4NO_3 from the PILS measurements. This approach assumes that the fine mode contains only sulfates, nitrates, and carbonaceous material. A plot of these three species is shown for the spring season in Figure 6. As stated before, the PILS measurements have been normalized to the 24-hr average data collected with the IMPROVE system, so if all of the assumptions were correct, the average TCM estimated in this fashion should compare to the TCM measured using the IMPROVE sampling system. With reference to the spring sampling period, the average of the TCM derived in this manner is 0.51 $\mu g/m^3$, whereas the average from the IMPROVE dataset is 0.97 $\mu g/m^3$ (POM + LAC). The IMPROVE TCM value is approximately 54% greater than that derived from the size distribution data. This difference could be because the IMPROVE $PM_{2.5}$ measurement of TCM contains some coarse-mode TCM; the R_{oc} multiplier for OC may be too high; the fine mode contains species other than SO_4^{2-}, NO_3^-, and POM; or all of the above. The agreement between IMPROVE reconstructed and measured $PM_{2.5}$ mass is somewhat improved when using a R_{oc} factor of 1.2, and the difference between the two TCM measurements drops to approximately 25%.

Referring to Figure 6, note that there is one episode on Julian day (JD) = 111 when NH_4NO_3 is over 6 $\mu g/m^3$ and other species concentrations are quite low. The episode on JD = 113 has about equal amounts of $(NH_4)_2SO_4$ and NH_4NO_3 at approximately 3 $\mu g/m^3$. $(NH_4)_2SO_4$ and NH_4NO_3 are elevated on JD = 115, with nitrates decreasing on JD = 116 and SO_4^{2-} staying at approximately 3 $\mu g/m^3$ through the end of the study period. POM concentrations are on the average lower than either sulfates or nitrates, with no notable episodes over the course of the measurement period.

The data for the summer campaign show quite different characteristics. First, it should be noted that although POM for the spring dataset makes up only 30% of the measured fine mass, during the summer that fraction is near 60%. For the summer dataset, the average TCM for the IMPROVE dataset is 3.44 $\mu g/m^3$, whereas for the NSD dataset it is 5 $\mu g/m^3$, a difference of approximately 30%. However, during the spring, the IMPROVE TCM value is greater than that derived from the NSD data. A scatterplot of summer IMPROVE TCM versus NSD TCM shows a high correlation of r = 0.97 and a slope of 1.27 ± 0.02, showing that although the correlation is high, NSD estimated from TCM is high by approximately 30%. Interestingly, when fine soil is added back into the fine mode (IMPROVE $PM_{2.5}$TCM + $PM_{2.5}$soil), the agreement between IMPROVE and what was assumed to be NSD TCM is much improved. The correlation is still high at 0.93, but the slope is 1.04 ± 0.03, showing that within the uncertainty the measurements are the same. Perhaps for this time period the soil elements found in the $PM_{2.5}$ mode are indeed in the fine mode and not the fine tail of the coarse mode. The POM during this time period was associated with major wildfire activity in the western United States. Others have reported[23] that there is a significant amount of soil-related elements during some types of fire activity. As with the inorganic variables, the excursions of TCM concentrations within a 24-hr interval are quite dramatic compared with the variability of 24-hr averages. During the summer campaign, the maximum TCM 24-hr average concentration was 11.5 $\mu g/m^3$, whereas for the NSD dataset it was 20.7 $\mu g/m^3$. The corresponding numbers for the spring dataset are 2 and 3.7 $\mu g/m^3$, about a factor of 2 in both cases.

Estimating Particle Extinction

The semicontinuous measured and derived speciated aerosol concentrations, along with normalized NSDs, can be used to estimate particle mass scattering/absorption efficiencies and atmospheric scattering and absorption. The fine and coarse modes as defined by the NSD measurements were treated as externally mixed from each other but uniformly mixed within each mode. Furthermore, on the basis of the above analysis, for spring the $PM_{2.5}$soil was assumed to be the fine tail of coarse mode soil, whereas during the summer $PM_{2.5}$soil was assumed to reside in the fine mode (<0.8 μm). Volume-weighted indices of refractions and densities were calculated based on the values of these variables listed in Table 6. Semicontinuous organic and EC concentrations for the spring were estimated using the average ratio of POM and LAC to TCM derived from the IMPROVE dataset. The POM/TCM ratio for spring was 0.91, whereas LAC/TCM was 0.09. For the summer dataset, the average IMPROVE fractions of $PM_{2.5}$soil, POM, and LAC to the total of these three variables were used to apportion NSD TCM to these three species. The fractions were 0.73, 0.22, and 0.05 for POM, soil, and LAC, respectively.

An estimation of $(NH_4)_2SO_4$ and NH_4NO_3 growth (D/Do) was calculated using the atoms in molecules (AIM)[24] "no solids" model (which assumes equilibrium below the crystallization point) over a range of 10–98% RH. AIM is an equilibrium thermodynamic model of the system H^+, NH_4^+, SO_4^{2-}, NO_3^-, and H_2O. The growth of the internally mixed soil-carbon-SO_4^{2-}/NO_3^- aerosol was then estimated using Zdanovskii-Stokes-Robinson (ZSR)[25] assumptions and aerosol densities presented in Table 6. ZSR assumptions imply that the amount of water a hygroscopic component brings into a mixture at some RH is equal to the amount of water it would have in a binary solution in equilibrium at the same RH. If it is assumed that in the internally mixed aerosol size distribution the chemical species are mixed in fixed proportions to each other across all sizes and the index of refraction is not a function of composition or size, the specific mass scattering efficiency can be prorated to the chemical constituents as if they were externally mixed on the basis of their relative densities using

$$e_{ik} = e_{mix}M_k/(m_{ik} + \rho_{ik}\sum_{j\neq i}(m_{jk}/\rho_{jk})) \quad (3)$$

where k is a specific sampling period; e_i and e_{mix} are the mass scattering efficiencies of species i and the mixed aerosol, respectively; M is the total mass; m_i and ρ_i are the mass and density of species i, respectively; and $\Sigma j \neq i$ is the sum over all species j not equal to i.

In Tables 9 and 10, *effs* and *effa* refer to hydrated mass scattering and absorption efficiencies, respectively, whereas b_{sp} and b_{abs} refer to the scattering and absorption

Table 9. Statistical summary of measured scattering and derived mass scattering and absorption coefficients for various species and estimated scattering/absorption associated with these species for spring.

Variable	Mean	SD	Minimum	Maximum	*N*
$effs_{fine}$	2.61	0.49	1.01	5.29	565
$effs_{so4}$	2.62	0.51	1.15	4.72	565
$effs_{no3}$	2.43	0.50	0.94	5.39	565
$effs_{POM}$	2.73	0.45	0.98	5.66	565
$effs_{LAC}$	2.12	0.35	0.76	4.40	565
$effs_{coarse}$	0.60	0.17	0.20	1.00	603
$effa_{fine}$	0.21	0.16	0.00	0.69	565
$effa_{coarse}$	0.00	0.00	0.00	0.00	603
b_{sp_so4}	3.43	4.26	0.10	34.43	565
b_{sp_no3}	1.29	3.45	0.00	25.61	565
b_{sp_POM}	1.26	1.48	0.00	10.47	565
b_{sp_LAC}	0.10	0.11	0.00	0.81	565
b_{sp_fine}	6.22	8.32	0.28	74.92	565
b_{sp_coarse}	1.84	1.50	0.02	8.40	603
b_{abs_fine}	0.37	0.54	0.00	9.23	565
b_{abs_coarse}	0.00	0.00	0.00	0.01	603
BF + BC/2	7.32	8.73	0.39	75.66	545
b_{sp}	9.12	10.33	−1.00	83.00	587
b_{ext}	8.67	9.39	0.53	85.63	545

Notes: Scattering and absorption efficiencies are in units of m^2/g; scattering and absorption are in Mm^{-1}.

coefficients, respectively. b_{sp} is measured scattering, and b_{ext} is estimated total fine plus coarse particle scattering plus absorption. $effs_{fine}$ is the mixed particle mass scattering efficiency, whereas subscripts of so4, no3, POM, LAC, soil, fine, and coarse refer to the mass scattering efficiencies associated with $(NH_4)_2SO_4$, NH_4NO_3, OC, LAC, soil, fine, and coarse mass concentrations. $BF + BC/2$ is just $b_{sp\_fine} + ½$ of coarse particle scattering, which should correspond to measured scattering, assuming that the nephelometer, on average, underestimated coarse particle scattering by a factor of 2.[26,27]

Figure 7, a and b, shows scatterplots of measured versus reconstructed fine particle plus ½ coarse particle scattering for the spring and summer datasets. In both cases, the coefficient of determination (R^2) is high at 0.80 and 0.91 for the spring and summer plots, respectively.

Table 10. Statistical summary of measured scattering and derived mass scattering and absorption coefficients for various species as well as estimated scattering/absorption associated with these species for summer.

Variable	Mean	SD	Minimum	Maximum	*N*
$effs_{fine}$	3.17	0.53	1.81	4.11	533
$effs_{so4}$	3.36	0.60	1.91	4.74	460
$effs_{no3}$	3.42	0.61	1.96	4.78	460
$effs_{POM}$	3.40	0.57	1.85	4.47	460
$effs_{soil}$	2.07	0.35	1.12	2.72	460
$effs_{LAC}$	2.50	0.42	1.43	3.23	533
$effs_{coarse}$	0.43	0.10	0.26	0.95	437
$effa_{fine}$	0.31	0.06	0.06	0.41	533
$effa_{coarse}$	0.10	0.07	0.00	0.28	437
b_{sp_so4}	5.23	3.04	0.88	20.59	460
b_{sp_no3}	1.40	2.57	0.10	29.41	460
b_{sp_POM}	14.33	8.51	0.93	52.96	460
b_{sp_soil}	2.01	1.19	0.13	7.41	460
b_{sp_LAC}	0.49	0.32	0.00	2.05	533
b_{sp_fine}	23.25	14.71	0.80	117.11	533
b_{sp_coarse}	2.24	1.52	0.08	10.73	570
b_{abs_fine}	2.26	1.33	0.02	8.56	533
b_{abs_coarse}	0.44	0.48	0.00	2.51	742
BF + BC/2	24.39	15.22	0.84	121.18	533
b_{sp}	20.66	14.29	0.00	135.00	570
b_{ext}	28.36	17.33	0.91	135.16	533

Notes: Scattering and absorption efficiencies are in units of m^2/g; scattering and absorption are in Mm^{-1}.

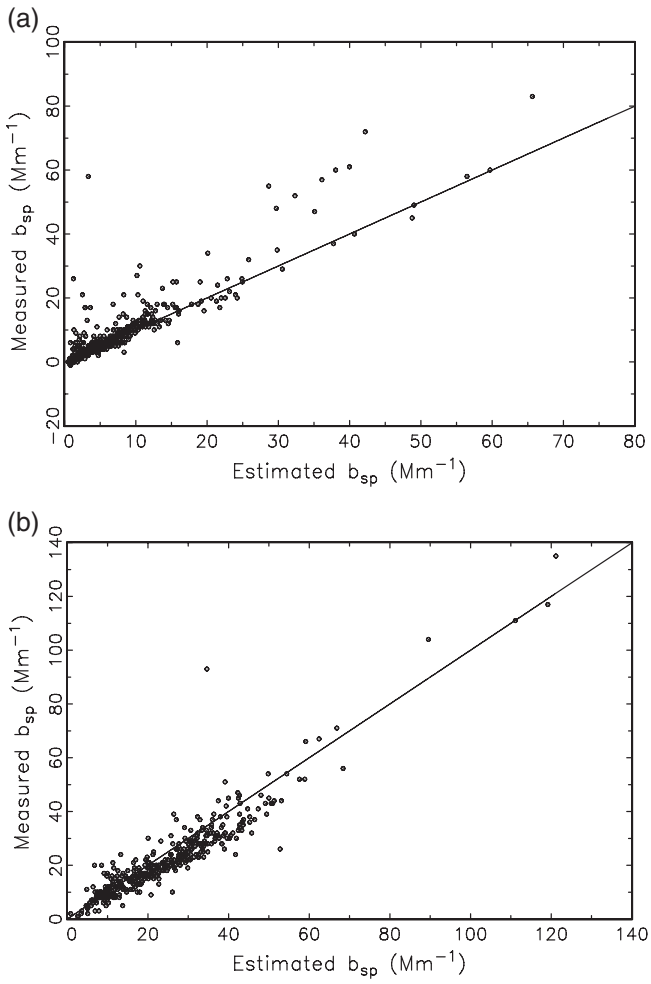

Figure 7. Scatterplots of reconstructed vs. measured fine + ½ coarse particle scattering for (a) spring and (b) summer measurement periods.

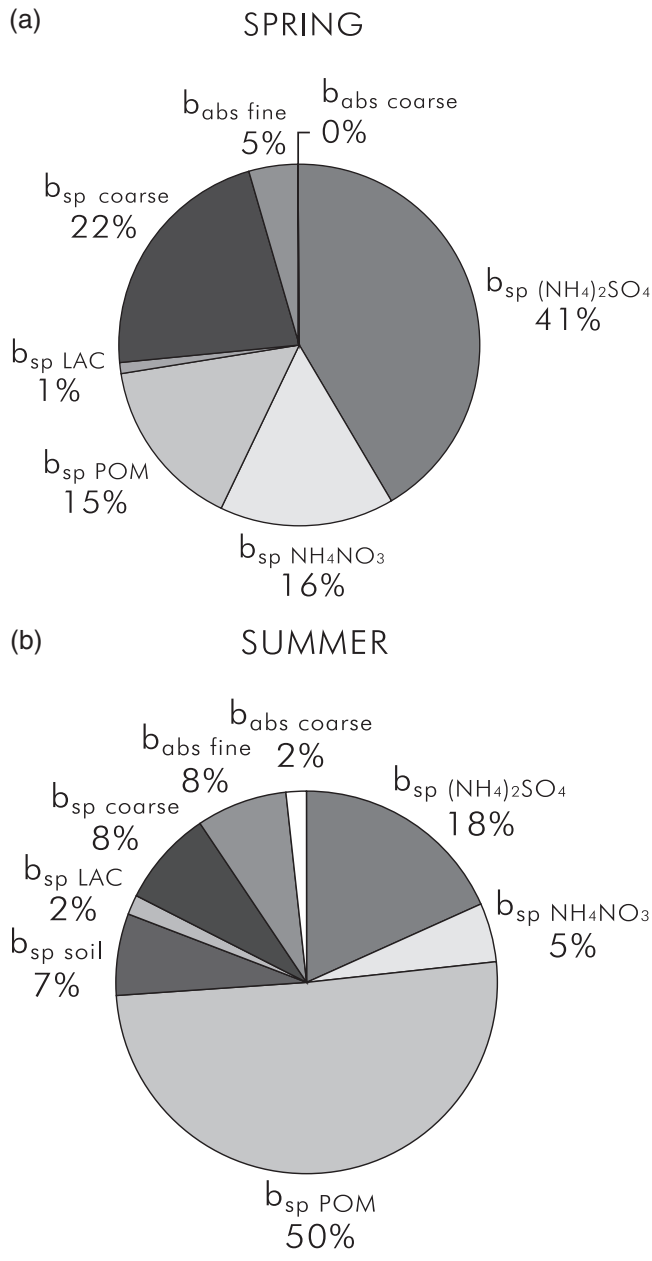

Figure 8. Approximate extinction budgets for (a) spring and (b) summer.

However, during the spring, measured scattering is on average higher than reconstructed scattering by approximately 20%, whereas during the summer it is lower by approximately 18%. During the spring, the agreement is quite good except for a few data points where the nephelometer-measured scattering was at times a factor of 2 higher than reconstructed scattering. The disagreement is greatest under the highest RH conditions, suggesting that the RH inside of the nephelometer may have been greater than at the RH sensor. During the summer, the agreement between measured and reconstructed scattering is quite good at lower scattering levels (<20 Mm^{-1}). At intermediate scattering levels ($20 < b_{sp\_fine} < 50$ Mm^{-1}); reconstructed scattering is systematically biased high by approximately 15–20%.

The mass scattering efficiencies for the spring dataset are generally lower than for summer by approximately 20%, primarily because summer size distributions are, on average, more narrow and have mass mean diameters more conducive to efficiently scatter light. The RH for the two sampling periods were about the same, with averages of 42 and 51% for spring and summer, respectively, and the highest humidities being approximately 95%. The average efficiency for the coarse mode was 0.43 during the spring and 0.60 during the summer.

The approximate particle extinction budgets for spring and summer are summarized in Figure 8, a and b. During the spring, $(NH_4)_2SO_4$ is the largest contributor to extinction at approximately 40%, with NH_4NO_3 and POM each contributing approximately 15% of overall extinction. Coarse mass scattering contributes another 22%, and particle absorption as the sum of fine and coarse absorption contributes another 5%.

During the summer, the average extinction budget is quite different. POM contributes 50% of the aerosol extinction, whereas $(NH_4)_2SO_4$ contributes another 18%. Coarse particle scattering was only 8%, and total fine plus coarse absorption was 10%.

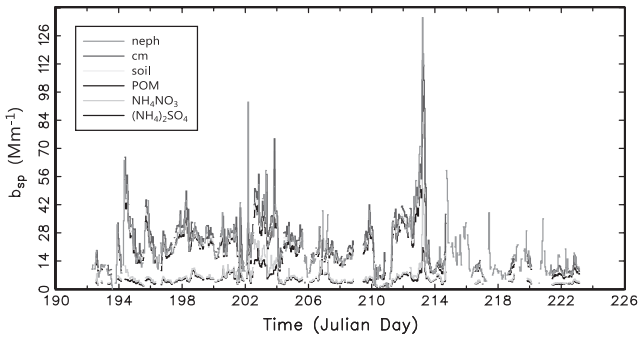

Figure 9. Temporal plot of measured and estimated atmospheric scattering of major aerosol species.

The average contribution of each species can be quite misleading in that averages can be made of up of extreme events. Figure 9 is a stacked temporal plot for the summer of the scattering contribution of each species and the nephelometer-measured atmospheric scattering coefficient. The variables are fine $(NH_4)_2SO_4$ and NH_4NO_3, POM, soil, and coarse mass. Notice that, as discussed previously, the large excursions in extinction can take place in time periods as short as hours. On the average, NH_4NO_3 only contributes approximately 5% of the extinction; however, on JD = 213 the NH_4NO_3 scattering coefficient is near 30 Mm^{-1}, which is more than 20% of total extinction. On a relative basis, nitrates are also high on JD = 194, 202, and 203; however, most hours NH_4NO_3 concentrations are very low and near the detection limit of the PILS monitoring system. The extreme event around 6:00 a.m. on JD = 213 corresponds to a nephelometer-measured aerosol scattering coefficient of 135 Mm^{-1}. If Rayleigh scattering and absorption are added to the measured scattering, the corresponding visual range is approximately 25 km. The corresponding lowest visual range during the spring season was approximately 40 km.

SUMMARY

RoMANS was designed to assess certain air quality issues in RMNP. As part of the study, an extensive monitoring program was carried out at one site, with a scaled-down set of measurements at secondary sites. At the central core site, measurements of 24-hr average $PM_{2.5}$ and PM_{10} gravimetric mass and $PM_{2.5}$ and PM_{10} SO_4^{2-}, NO_3^-, POM, LAC, and soil-related elements were made. Semicontinuous measurements were also made of SO_4^{2-}, NO_3^-, particle size distributions from 0.05 to 15 μm, and atmospheric scattering. Redundant and related measurements were compared to identify biases, estimate errors, and assess the overall suitability of the data for the various analyses.

The semicontinuous measurements of SO_4^{2-} and NO_3^- concentrations compared favorably to the $PM_{2.5}$ 24-hr average measurements, with differences being on the order of 25–40% and 5–15% during the summer and spring, respectively. For the purposes of calculations carried out in the analysis presented here, the semicontinuous inorganic ion data were normalized to the 24-hr average measurements.

$PM_{2.5}$ concentrations were about a factor of 2 higher in the summer than spring, primarily because of increased concentrations of POM. However, as might be expected, springtime NO_3^- concentrations also exceeded those of the summer season by about a factor 2. During the spring, $PM_{2.5}$ sulfates, nitrates, POM, and soil elements contributed about equally to $PM_{2.5}$ mass concentrations, whereas during the summer, POM was the largest contributor at 60%. During spring and summer, $PM_{10} - PM_{2.5}$ was made up primarily of soil elements at approximately 75%, whereas POM was the second largest contributor at 15–20%.

The most striking feature of the semicontinuous data is the extreme, short-time-scale variability aerosol concentrations. Typically, any 24-hr bulk measured concentration is made up of short-term episodes that are 12 hr or less in duration. For instance, the 24-hr average maximum NO_3^- concentration for the spring is 1.48 $\mu g/m^3$, whereas the maximum 1-hr concentration is 4.95 $\mu g/m^3$, a factor of 3.3 higher. Sulfates and POM show similar short-time-scale variability for the spring and summer datasets.

The average densities of the fine and coarse modes were calculated in two ways. First, a volume-weighted calculation using measured aerosol species and known densities was carried out; second, an average density was estimated from the slope of a scatterplot between measured mass and corresponding volume derived from particle size distribution measurements. The relative errors between the two calculations for PM_{10} volumes and mass concentrations were 6 and 9% for the spring and summer months, respectively, with the volume-weighted density being smaller in the spring but larger in the summer. Interestingly, the relative errors for the individual fine and coarse modes were less at approximately 1–6%. An interesting observation was that although the spring dataset $PM_{2.5}$soil may correspond to the fine tail of the $PM_{10}-PM_{2.5}$soil, during the summer the $PM_{2.5}$soil is likely in the fine mode (0.05–0.8 μm).

Total semicontinuous fine mode (0.05–0.8 μm) carbonaceous mass (TCM = POM + LAC) was estimated by differencing the mass concentrations derived from the NSD measurements and the sum of $(NH_4)_2SO_4$ and NH_4NO_3 from the PILS measurements, assuming that all sulfates, nitrates, and POM occurred only in the fine mode.

The semicontinuous measured and derived speciated aerosol concentrations were used to derive semicontinuous estimates of fine and coarse mode indices of refraction and densities, which when combined with the NSD data allowed for estimations of particle mass scattering/absorption efficiencies and atmospheric scattering and absorption.

The average RH for the spring and summer time frames were about the same; however, the mass scattering efficiencies were approximately 20% higher during the summer because size distributions were, on the average, narrower and therefore more conducive to efficiently scatter light.

During the spring, average extinction was estimated to be approximately 9 Mm^{-1}, with sulfates on the average contributing 40% of the extinction and coarse mass contributed another 22%. NH_4NO_3 and POM both contributed on the order of 15%. During the summer, the average extinction was 28 Mm^{-1}, with POM contributing approximately 50% and $(NH_4)_2SO_4$ contributing another

22%. Contributions of other species to total extinction were all less than 10%.

The average contribution of each species can be quite misleading in that averages can be made of up of extreme events. Large excursions in extinction can take place in time periods as short as hours. On the average, NH_4NO_3 only contributes approximately 5% of the extinction; however, on JD = 213 the NH_4NO_3 scattering coefficient is near 30 Mm^{-1}, which is more than 20% of total extinction. On the highest extinction hours, the corresponding visual ranges are approximately 25 and 40 km for the summer and spring, respectively.

ACKNOWLEDGMENTS

The assumptions, findings, conclusions, judgments, and views presented herein are those of the authors and should not be interpreted as necessarily representing the National Park Service policies.

REFERENCES

1. Yu, X.-Y.; Lee, T.; Ayres, B.; Kreidenwies, S.M.; Collett, J.L., Jr. Particulate Nitrate Measurement Using Nylon Filters; *J. Air & Waste Manage. Assoc.* **2005**, *55*, 1100-1110.
2. Yu, X.-Y.; Lee, T.; Ayres, B.; Kreidenweis, S.M.; Collett, J.L., Jr. Loss of Fine Particle Ammonium from Denuded Nylon Filters; *Atmos. Environ.* **2006**, *40*, 4797-4807.
3. Orsini, D.A.; Ma, Y.L.; Sullivan, A.; Sierau, B.; Baumann, K.; Weber, R.J. Refinements to the Particle-into-Liquid Sampler (PILS) for Ground and Airborne Measurements of Water Soluble Aerosol Composition; *Atmos. Environ.* **2003**, *37*, 1243-1259.
4. Sorooshian, A.; Brechtel, F.J.; Ma, Y.L.; Weber, R.J.; Corless, A.; Flagan, R.C.; Seinfeld, J.H. Modeling and Characterization of a Particle-into-Liquid Sampler; *Aerosol Sci. Technol.* **2006**, *40*, 396-409.
5. Weber, R.; Orsini, D.; Duan, K.; Baumann, C.S.; Kiang, W.; Chameides, Y.N.; Lee, F.; Brechtel, P.; Klotz, P.; Jongejan, H.; ten Brink, J.; Slanina, C.B.; Boring, Z.; Genfa, P.; Dasgupta, S.; Hering, M.; Stolzenburg, D.D.; Dutcher, E.; Edgerton, B.; Hartsell, B.; Solomon, P.; Tanner, R. Intercomparison of Near Real Time Monitors of $PM_{2.5}$ Nitrate and Sulfate at the U.S. Environmental Protection Agency Atlanta Supersite; *J. Geophys. Res. Atmos.* **2003**, *108*, 8421, doi: 10.1029/2001JD001220.
6. Hering, S.V.; McMurry, P.H. Response of a PMS LAS-X Laser Optical Counter to Monodisperse Atmospheric Aerosols; *Atmos. Environ.* **1991**, *25*, 463-468.
7. Sachweh, B.; Umhauer, H.; Ebert, F.; Buttner, H.; Friehmelt, R. In Situ Optical Particle Counter with Improved Coincidence Error Correction for Number Concentrations up to 10^7 Particles cm^{-3}; *J. Aerosol Sci.* **1998**, *29*, 1075-1086.
8. Armendariz, A.J.; Leith, D. Concentration Measurement and Counting Efficiency for the Aerodynamic Particle Sizer 3320; *J. Aerosol Sci.* **2002**, *33*, 133-148.
9. Hand, J.L.; Kreidenweis, S.M.; Sherman, D.E.; Collett, J.L., Jr.; Hering, S.V.; Day, D.E.; Malm, W.C. Aerosol Size Distributions and Visibility Estimates during the Big Bend Regional Aerosol and Visibility Observational (BRAVO) Study; *Atmos. Environ.* **2002**, *36*, 5043-5055.
10. McMeeking, G.; Kreidenweis, S.M.; Carrico, C.M.; Lee, T.H.; Carrillo, J.; Collett, J.L., Jr.; Day, D.E.; Hand, J.L.; Malm, W.C. Dry Aerosol Size Distributions and Derived Optical Properties during the Yosemite Aerosol Characterization Study; Presented at the Air & Waste Management Association Specialty Conference, Asheville, NC, 2004.
11. Hand, J.L.; Malm, W.C. Review of Aerosol Mass Scattering Efficiencies from Ground-Based Measurements since 1990; *J. Geophys. Res.* **2007**, *112*, D16203, doi: 10.1029/2007JD008484.
12. Malm, W.C.; Sisler, J.F.; Huffman, D.; Eldred, R.A.; Cahill, T.A. Spatial and Seasonal Trends in Particle Concentration and Optical Extinction in the United States; *J. Geophys. Res.* **1994**, *99*, 1347-1370.
13. Hand, J.L.; Kreidenweis, S.M. A New Method for Retrieving Particle Refractive Index and Effective Density from Aerosol Size Distribution Data; *Aerosol Sci. Technol.* **2002**, *36*, 1012-1026.
14. Stolzenburg, M.; Kreisberg, N.; Hering, S. Atmospheric Size Distributions Measured by Differential Mobility Optical Particle Size Spectrometry; *Aerosol Sci. Technol.* **1998**, *29*, 402-418.
15. Malm, W.C.; Pitchford, M.L. Comparison of Calculated Sulfate Scattering Efficiencies as Estimated from Size-Resolved Particle Measurements at Three National Locations; *Atmos. Environ.* **1997**, *31*, 1315-1325.
16. Ames, R.B.; Hand, J.L.; Kreidenweis, S.M.; Day, D.E.; Malm, W.C. Optical Measurements of Aerosol Size Distributions in Great Smoky Mountains National Park: Dry Aerosol Characterization; *J. Air & Waste Manage. Assoc.* **2000**, *50*, 665-676.
17. Malm, W.C.; Day, D.E.; Kreidenweis, S.M. Optical Properties of Aerosols at Grand Canyon National Park; *J. Air & Waste Manage. Assoc.* **2000**, *50*, 686-700.
18. Tang, I.N. Chemical and Size Effects of Hygroscopic Aerosols on Light Scattering Coefficients; *J. Geophys. Res.* **1996**, *101*, 19245-19250.
19. Dick, W.D.; Saxena, P.; McMurry, P.H. Estimation of Water Uptake by Organic Compounds in Submicron Aerosols Measured during the Southeastern Aerosol and Visibility Study; *J. Geophys. Res.* **2000**, *105*, 1471-1479.
20. Stelson, A.W. Urban Aerosol Refractive Index Prediction by Partial Molar Refraction Approach; *Environ. Sci. Technol.* **1990**, *24*, 1676-1679.
21. Seinfeld, J.H.; Pandis, S.N. *Atmospheric Chemistry and Physics: from Air Pollution to Climate Change*; John Wiley: New York, 1998.
22. Malm, W.C.; Pitchford, M.L.; McDade, C.E.; Ashbaugh, L.L. Coarse Particle Speciation at Selected Locations in the Rural Continental United States; *Atmos. Environ.* **2007**, *41*, 2225-2239.
23. Allen, A.G.; Miguel, A.H. Biomass Burning in the Amazon: Characterization of the Ionic Component of Aerosols Generated from Flaming and Smoldering Rainforest and Savannah; *Environ. Sci. Technol.* **1995**, *29*, 486-493.
24. Clegg, S.L.; Brimblecombe, P.; Wexler, A.S. Thermodynamic Model of the System H^+–NH_4^+–Na^+–SO_4^{2-}–NO_3^-–Cl^-–H_2O at 298.15 K; *J. Phys. Chem.* **1998**, *102A*, 2155-2171.
25. Saxena, P.; Peterson, T.W. Thermodynamics of Multicomponent Electrolytic Aerosols; *J. Colloid Interface Sci.* **1981**, *79*, 496-510.
26. Hasan, H.; Lewis, C.W. Integrating Nephelometer Response Corrections for Bimodal Size Distributions; *Aerosol Sci. Technol.* **1983**, *2*, 443-453.
27. White, W.H.; Macias, E.S.; Ninger, R.C.; Schorran, S. Size-Resolved Measurements of Light Scattering by Ambient Particles in the Southwestern U.S.A.; *Atmos. Environ.* **1994**, *28*, 909-921.

About the Authors

William Malm is a research physicist with the National Park Service Air Resources Division in Fort Collins, CO. Sonia Kreidenweis is a professor, Ezra Levin is a graduate student, Christian Carrico is a research scientist, Jeffrey Collett, Jr. is a professor, Taehyoung Lee is a research scientist, and Amy Sullivan is a research scientist with the Department of Atmospheric Science at Colorado State University (CSU) in Fort Collins, CO. At the time of the work, Gavin McMeeking was a graduate student and Suresh Raja was a postdoctoral fellow with the Department of Atmospheric Science at CSU. Gavin McMeeking is now a postdoctoral fellow at the University of Manchester, England, and Suresh Raja is now a research assistant professor at Clarkson University in Potsdam, NY. Derek Day is a research associate with the Cooperative Institute for Research in the Atmosphere at CSU in Fort Collins, CO. Please address correspondence to: William Malm, National Park Service, Cooperative Institute for Research in the Environment, Colorado State University, 1375 Campus Delivery, Fort Collins, CO 80523; phone: +1-970-491-8292; fax: +1-970-491-8598; e-mail: malm@cira.colostate.edu.